Design and Analysis of Ultra-Miniaturized Meandering Photonic Crystals Delay Lines

Mohammad Fakharzadeh, Omar M. Ramahi, Safiedin Safavi-Naeini, and Sujeet K. Chaudhuri

***Abstract*—In this paper, we study the characteristics of a novel miniaturized optical delay line, which delays light in a meandering photonic crystal waveguide, and describe the design steps. We show how lattice parameters and refractive index difference of the photonic crystal affect the bandgap width and suggest a criterion to select these parameters. Next, we focus on the parallel waveguide channels in photonic crystal, and analyze the impact of the channel length and the interchannel spacing on crosstalk. We suggest a method for mitering the sharp corners in meandering lines which reduces the undesired reflections by 8 dB. Considering all these guidelines, we examine the propagation of light in the proposed delay line through calculating time-delay and insertion loss. To achieve longer delays in a small device area, we concentrate on coupled cavities in photonic crystals and propose an approximate method for calculating the group velocity of light in the coupled defects. We show how by replacing waveguide channels of a meandering delay line with coupled defects we achieve time-delays more than 9 ps within a device size around 27 μm, which corresponds to a miniaturization factor of 100.**

***Index Terms*—Coupled cavities, crosstalk, finite difference time domain (FDTD), group velocity, optical delay line, photonic crystal.**

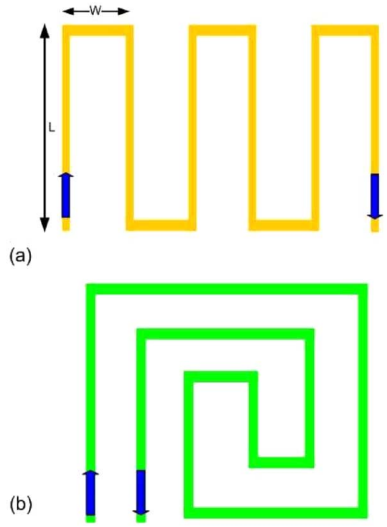

Fig. 1. Two types of meandering line structures. (a) Serpentine. (b) Double spiral.

I. Introduction

OPTICAL delay lines (ODLs) are widely used in numerous applications, such as broadband beamforming of phased array systems, optical division multiplexing, filter design and optical signal processing. Traditionally, optical fibers have been used as the main element of the ODL, because fiber is a low loss medium and supports the propagation of large bandwidth signals. Use of long lengths of fiber to generate large time delays is unavoidable, however, for short time delays (<1 μs), still long pieces of fiber are required. For example, Chang *et al.* [1] used a 940 m graded index multimode fiber as delay line to generate 4.99 μs/km delay. Such delay lines are heavy, lossy, and bulky, furthermore, integration of long lengths of fiber with other optical subsystems is not practical.

A solution to achieve compact delay lines, which appeared in the early 1990s, was the use of fiber Bragg grating instead of regular single mode fibers. For example, Ortega *et al.* [2] introduced an ODL with a maximum delay of 330 ps for a 5 cm uniform grating. The performance of such delay lines is only two times better than free space in terms of the required propagation length, so still the packaging and integration problems exist.

Use of photonic crystal (PC) is a promising solution to reduce the size of delay elements. Very small group velocities are achievable at the band edges of PCs [3], and bandgap mechanism slows down the propagation of light. The crystal can confine light around sharp bends, in lower-index media, and within wavelength-scale cavities. The other important advantage of PC is that it can be integrated with silicon-on-insulator (SOI) and CMOS devices to achieve a low cost product. Recently, many works have been reported on the design and fabrication of photonic crystal devices, specifically delay lines [4]–[10]. However, all of these works, use *straight* line structures in PC, so to achieve longer time delays, the device size must be increased.

In this paper, the main focus is on the design and analysis of *meandering* photonic crystal delay lines. We have proposed carving meandering line structures in photonic crystals to make delay lines [11]. Meandering line structures have a high packing density which results in a more efficient use of the device area. General meandering lines consist of parallel waveguides connected with crossed interconnections. Two conventional arrangements for this category of delay lines, which are used in microwave frequencies, are serpentine (meander) and double spiral. Fig. 1 illustrates the geometry of these two delay lines. We will focus on two different structures

Manuscript received July 5, 2007; revised September 20, 2007. This work was supported by an industrial research chair program sponsored by Research In Motion (RIM) and Natural Sciences and Engineering Research Council of Canada (NSERC). This work was recommended for publication by Associate Editor L.-T. Hwang upon evaluation of the reviewers comments.

The authors are with the Electrical and Computer Engineering Department, University of Waterloo, Waterloo, ON N2L 3G1, Canada (e-mail: mfakharz@uwaterloo.ca).

Color versions of one or more of the figures in this paper are available online at http://ieeexplore.ieee.org.

Digital Object Identifier 10.1109/TADVP.2008.916284

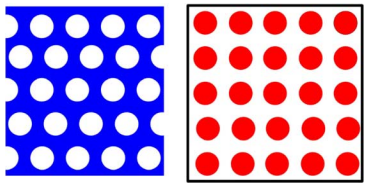

Fig. 2. Top view of two conventional structures for 2-D photonic crystals. Left: Triangular lattice. Right: Square lattice.

to implement ODLs in photonic crystals: 1) waveguide-based delay lines and 2) coupled cavity (defect) delay lines.

The organization of this paper is as follows. In Section II, we discuss the design steps of a meandering delay line in PC. We propose a criterion for selecting the lattice parameters, and show how crosstalk between parallel waveguides can be reduced by choosing appropriate dimensions for waveguide channels. In Section III, we introduce reflective spiral delay line and use full-wave analysis to examine its characteristics. In Section IV, we discuss coupled cavity delay lines and illustrate that replacing PC waveguides with coupled cavities can significantly increase the time delay and decrease the insertion loss. Finally, in Section V, we present the conclusions of this paper.

II. Design Steps for Photonic Crystal Delay Lines

Photonic crystals, also known as photonic bandgap (PBG) material, are structures with a periodically modulated dielectric material constant. If the depth of the refractive index modulation is adequate, there will be a certain frequency range, namely *bandgap*, where optical modes are forbidden to propagate. PCs are divided into three types according to the dimensionality of their periodicity, namely 1-D, 2-D, and 3-D PCs. In reality dimensions of a PC structure are limited and the periodicity is terminated at some point. Instead of using fictitious 2-D or 3-D PCs, photonic crystal slabs have been proposed as a more easily fabricated alternative to 3-D PCs. PC slabs are 2-D periodic dielectric structures of finite height with a band gap for propagation in the plane of periodicity. The index-confinement is used for guiding light in the third dimension. PC slabs are also called quasi-2-D PCs because their structure and properties imitates those of 2-D PCs [12]. Since the fullwave analysis of 3-D structures is time-consuming and needs significant amount of memory, we focus on 2-D structures in the rest of this paper.

A. Photonic Crystal Structures

Amongst different periodic structures for 2-D PCs, two structures have been more popular named *triangular* and *square* lattice which are demonstrated in Fig. 2. Each of these structures can be obtained by embedding rods of a high-index material in a low-index medium or drilling holes in a high-index medium. These holes are filled with a low-index material like air or silica (SiO_2). Triangular lattice PCs support both TE and TM modes, where in TM modes H-field is parallel to the rods, while in TE modes E-field has this property. Square-lattice PCs only support TE modes but they generally possess a wider bandgap compared to triangular structures. In the rest of this work, we focus on square-lattice PCs consisting of high-index cylinders. To specify

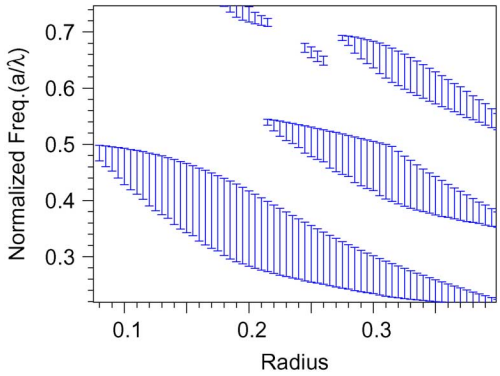

Fig. 3. Gap map for the square lattice of silicon rods in air.

this structure completely, we need to find the material, the radius of cylinders, R_0, and the lattice constant, a, which is defined as the distance between centers of the adjacent cylinders. Choosing high and low index material is restricted to the current technology and the available transparent material with lossless optical propagation. Usually Si ($n = 3.45$) or GaAs ($n = 3.4$) is used as the high-index material and air ($n = 1$) or silica ($n = 1.45$) is used as the low-index medium [13]. We start with Si/Air configuration and discuss other material later.

B. Finding Lattice Constant and Radius

Existence of the bandgap and the width of the bandgap depend on the ratio of rod radius over lattice constant, R_0/a. Due to the scaling property of Maxwell equations, as long as the material properties remain the same, solving a problem at one length scale determines the solutions at other length scales [21]. Therefore, we initially fix a at 1 μm and vary R_0 from $0.05a$ to $0.40a$ in steps of $0.005a$. We use the plane wave expansion method to find the bandgap for each value of R_0. Eventually, a graph like Fig. 3 is achieved. This graph is called gap-map and conveys important information for design of PBG devices. Fig. 3 shows that the maximum bandgap for Si/Air configuration occurs for $R_0 = 0.18a$. Having the widest bandgap is an appropriate criterion for setting lattice parameters, because it compensates for the fabrication errors and uncertainties, and enables the design of a wide-band device. The vertical axis in Fig. 3 shows the normalized frequency represented by a/λ. If we want to design a photonic crystal waveguide to transmit a modulated optical signal, it is wise to set the center frequency equal to the optical carrier frequency. Therefore, even for ultra-wideband signals, a negligible fraction of the power will be absorbed. For this configuration, the widest bandgap is centered at $a/\lambda = 0.37$. So, for the optical communication wavelength of $\lambda = 1.55$ μm the lattice constant will be $a = 574$ nm, and the cylinder's radius, R_0 is 103 nm.

Further analysis shows as Δn, the refractive index difference of the material which constitute the PC, increases the bandgap widens and its center approaches lower frequencies. The reverse happens if Δn decreases. Fig. 4 demonstrates the gap-map for Si/SiO_2 configuration where $\Delta n = 2$. The widest bandgap occurs for a larger ratio of R_0/a compared to Air/Si configuration (0.226 instead of 0.18).

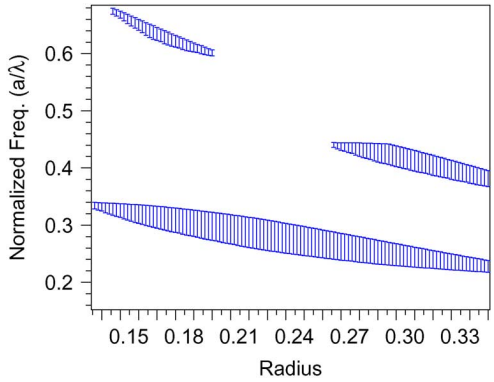

Fig. 4. Gap map for the square lattice of silicon rods in SiO_2.

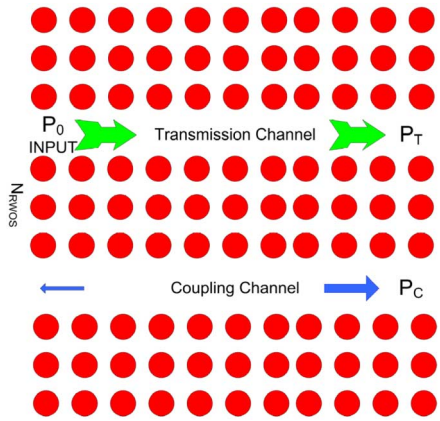

Fig. 5. Basic structure used as the test-bed for the coupling analysis in parallel PC waveguides.

C. Crosstalk Reduction

Crosstalk is a major drawback of meandering delay lines. If we place the vertical channels in the delay lines of Fig. 1 as close as possible and increase their length, the propagation path enlarges. However, fast coupling between parallel lines (or crosstalk) limits the maximum length of the lines and the minimum distance between the adjacent lines. Crosstalk between the parallel photonic crystal waveguides (PCW) has been discussed in [14]–[19]. In these earlier works the interest was mostly on analyzing the variation of coupling versus wavelength or finding the coupling length. Here, we study the effects of the channel length and spacing variations to tradeoff between crosstalk and packing density of waveguide channels. Indeed, we have two incompatible goals, we want to: 1) keep the crosstalk between parallel channels as low as possible to assure that light is transferred only through propagation and 2) use the device area efficiently by placing waveguide channels as close as possible. We use the finite difference time domain (FDTD) method to study the propagation of light in the PC waveguide channels. Fig. 5 shows the test-bed used for the current studies, which consists of the silicon rods suspended in air. This structure is the PC equivalent of a microwave directional coupler. Transmission chancel in Fig. 5 is the forward path that transfers energy from the source to the output. Coupling channel is a parallel path without any independent source that is excited through coupling of energy. N_R denotes the number of rows or the distance between these two channels ($N_R = 1, 2, \ldots, \infty$). We use pulse excitation as the input to the system under test and measure (record) the amplitude or envelope of the electric field at the desired points. The excitation pulse consists of a Gaussian envelope modulation on a sinusoidal carrier

$$p(t) = \exp\left[-\left(\frac{t}{\tau - t_0}\right)^2\right] \sin\left(\frac{2\pi}{\lambda}t\right) \tag{1}$$

where τ is pulse width, t_0 is the initial delay, and λ is the center wavelength of the pulse.

For the following set of simulations τ in (1) is equal to 15 cycles of the carrier wave. This setting would concentrate most of the transmitted energy in a bandwidth equal to 4 THz, provided that the center wavelength, λ is set to 1.55 μm. To find the best channel spacing, we fix the channel length (L) at 25μm and calculate the instantaneous power at the input port, P_0 and at the output of the transmission and coupling channels, respectively, denoted by P_T and P_C. Then by integrating P_T and P_C over time, we find the total transmitted and coupled energy. Hence, two parameters namely transmittance (T) and coupling (C) factors are defined

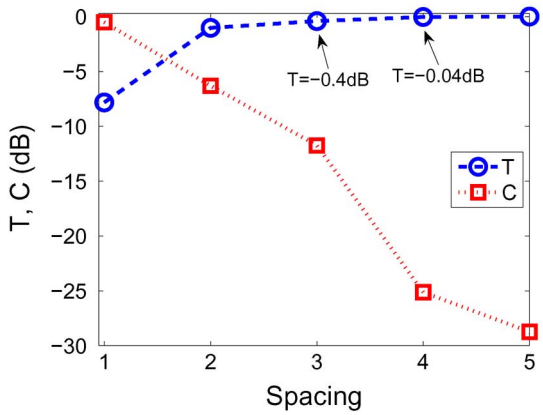

Fig. 6. Transmittance and coupling factors for different interchannel spacings. L, the channel length is 25 μm.

$$T = \frac{\int P_T(t)dt}{\int P_0(t)dt} \tag{2}$$

and

$$C = \frac{\int P_C(t)dt}{\int P_0(t)dt}. \tag{3}$$

Fig. 6 presents the calculated transmittance and coupling factor for $1 \leq N_R \leq 5$. we observe that for $N_R = 3$, the transmittance is $T = -0.4$ dB which means more than 91% of the input energy directly transmits and the rest is coupled to the coupling channel, absorbed into the crystal (due to the large bandwidth of the source signal), or reflected back to the input port. For $N_R = 4$, the transmittance increases to $T = -0.04$ dB which means 99% of the input energy is transmitted in the desired channel, so we conclude that $N_R \geq 4$ is a proper choice for the interchannel spacing in the meandering PC structures.

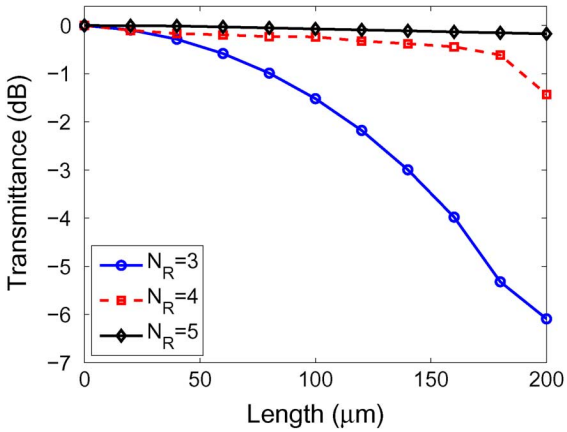

Fig. 7. Transmittance versus channel length ($\lambda_0 = 1.55\ \mu\mathrm{m}$). By increasing the spacing between parallel channels transmittance increases and crosstalk decreases.

Crosstalk also depends on channel length, and for sufficiently long parallel waveguides, it has a periodic behavior versus length. To study the effect of the channel length on crosstalk of parallel waveguide channels in PC, we use a test-bed structure similar to Fig. 5 with the same excitation. The channel spacing, N_R alters from 3 to 5, and the channel length, L, varies from 10 to 200 μm. Fig. 7 illustrates the FDTD results. It is seen that for $N_R = 3$ Transmittance decreases dramatically as L rises, however for $N_R = 4$, the drop in T is smoother and even negligible for $N_R = 5$. Since we want to achieve long delays with low insertion loss, for the rest of this paper we consider five layers of Si rods between parallel waveguide channels. Notice that these results are based on 2-D FDTD simulations which does not support scattering loss calculations. In reality the limited length of Si rods (or air holes) in PC results in scattering loss. Fortunately, by refractive index confinement, we are able to reduce the out-of-plane loss of PC waveguides. Wan Kuang *et al.* [17] used 3-D fullwave simulations to show low loss propagation in the PC waveguides with index-confinement is possible.

D. Corner Mitering

A meandering path, which is our desired structure for delay line consists of several sharp bends which are made to increase the net propagation length of light. Initially, the exclusive possibility of making sharp bends in PC, stimulated us to develop meandering PC channels. However, it is necessary to miter all corners to reduce the reflection from each corner, otherwise a large part of the input power will be lost through multiple corner reflections. Fig. 8 graphically shows the method we used for mitering corners [18]. We shift three rods at the corner diagonally, and reduce their radii according to the values shown in the figure. Fig. 9 compares the reflection coefficient for two successive corners in a meandering line carved in PC before and after mitering. It is shown that after mitering the reflection coefficients reduce by at least 8 dB. Therefore, to achieve low loss delay lines, corner mitering in meandering PC structures is unavoidable.

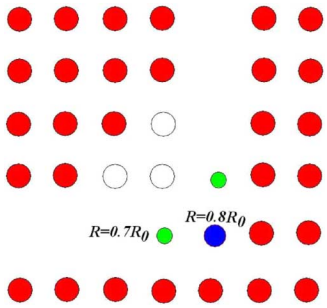

Fig. 8. Method used for mitering.

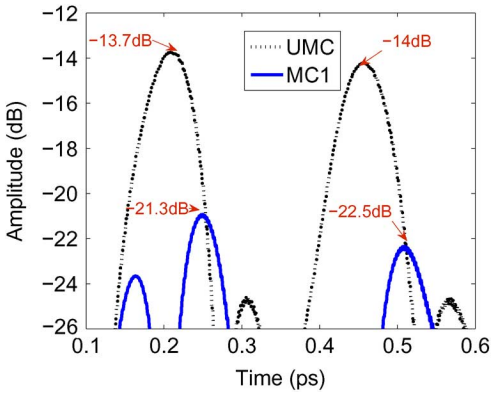

Fig. 9. Reflection from two corners. UMC: Unmodified corners. MC: Mitered corners.

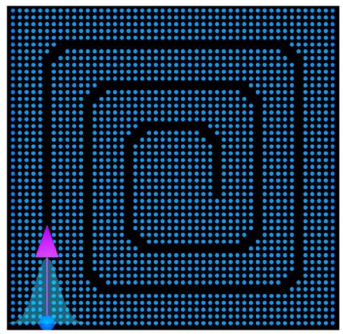

Fig. 10. Top view of Reflective Spiral Line carved in a square lattice PC.

III. Reflective Spiral Line in Photonic Crystal

In transmission line theory, an open-circuit termination causes total reflection, so the forward travelling wave totally returns toward the input terminal. Similarly, in a well-designed PC waveguide the walls behave like mirrors which can reflect lightwave [21]; so, if one puts a mirror at the end of the waveguide, all of the travelling lightwave will return. This concept becomes realizable by removing a certain number of cells in a PBG lattice to open a channel and stopping at some point which is adequately far from the boundaries. The closed end of the channel behaves exactly like a mirror for the wavelengths inside the bandgap, with a reflection coefficient close to 1. Fig. 10 shows the implementation of this idea in photonic crystal. We have introduced the *novel* structure arising from this arrangement, henceforth called *reflective spiral line* in [11], for the first time. As mentioned in the previous section,

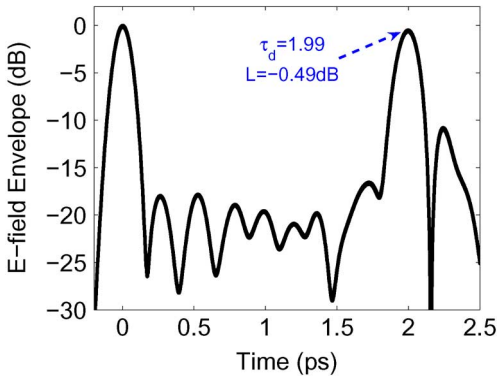

Fig. 11. Envelope of the electric field detected at the input/output of the Si/Air reflective spiral delay line.

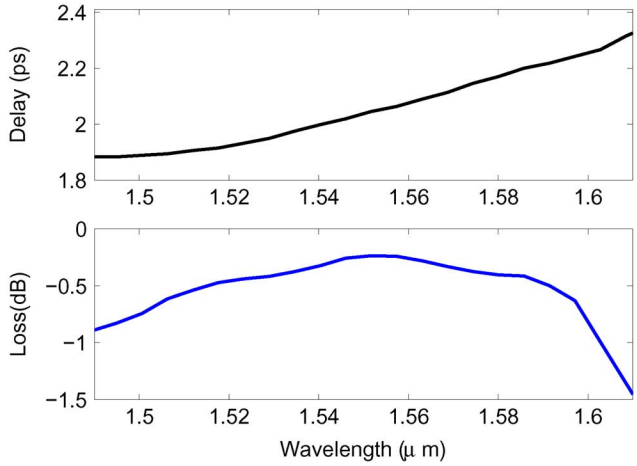

Fig. 12. Delay and loss versus wavelength for Reflective Spiral Line.

to reduce the crosstalk, we fix N_R at 5 and channel lengths are less than 21 μm. Since reflective spiral line is a single port device, an optical circulator will be required to separate input and output signals. In [22], an optical circulator formed by inserting magneto-optical cavity in a 2-D PC is proposed.

Fig. 11 shows the envelope of the electric field recorded at the input/output of this delay line. We define *delay* as the time difference between the maximum of the input pulse envelope, centered at $t = 0$, and the maximum of the pulse response recorded at the output terminal. *Loss* is defined as the ratio of the electric field amplitudes at these two points. These are two qualitative criteria to facilitate the comparison of different structures. The FDTD simulations show that the time-delay of this structure is 1.99 ps and the loss is less than 0.3 dB. The largest device size, including the margins, is only $L = 27$ μm.

To provide a meaningful comparison of the time delay relative to the device size, we define a figure of merit for delay F_d, as

$$F_d = c\frac{\tau_d}{L} \tag{4}$$

where c is the speed of light in free space, τ_d is the time delay, and L is the device size. This figure of merit simply states how many times light can be slowed down in this structure compared to free space. The effect of the meandering shape is also included in F_d. For the delay line displayed in Fig. 10, we can show that $F_d = 22.2$. In [11], we have compared reflective spiral structure with conventional structures for delay lines, i.e., meandering line and double spiral line. We have shown that the performance of this delay line in terms of the propagation delay, loss, and cross talk is at least two times better than other structures with the same device size.

Further analysis shows that the generated delay in reflective spiral structure increases as the optical carrier frequency increases (Fig. 12). For example, if we change the wavelength from 1.49 μm to 1.61 μm—almost 8%— the time delay increases by 25%. However the propagation loss decreases as the wavelength approaches the center wavelength (1.55 μm) and after that it increases.

If we want to implement the same structure with Si/SiO_2, configuration we have to change the lattice parameters. As Fig. 4 illustrates, for this case the maximum bandgap occurs for $R_0 = 0.226a$. The bandgap is centered at $a/\lambda = 0.284$, thus for $\lambda_0 = 1.55$ μm, a and R_0 are found to be 440 and 100 nm, respectively. This time the lattice constant is smaller than that of Si/Air configuration, so the length of the Si/SiO_2 reflective spiral delay line will be smaller by a scaling factor corresponding to the ratio of the lattice constants of both structures. Fig. 13 demonstrates the envelope of the electric field recorded at the input/output of the Si/SiO_2 reflective spiral delay line. We observe that both delay and loss have increased to 2.21 ps and 3.3 dB, respectively, however the device size has shrunk to 20.7 μm. Therefore, $F_d = 32.05$ for Si/SiO_2 reflective spiral delay line, which implies that the propagation of light Si/SiO_2 PC delay line is 1.45 times slower than Si/Air configurations.

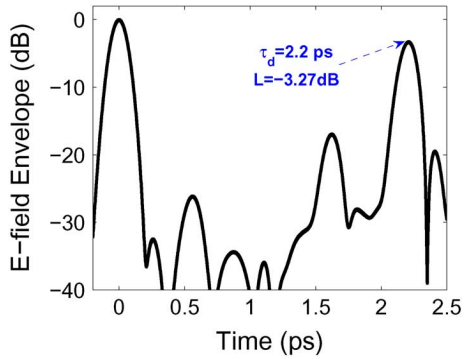

Fig. 13. Envelope of the electric field detected at the input/output of the Si/SiO_2 reflective spiral delay line.

IV. Coupled Cavities in Photonic Crystals

A cavity in a PC is a modified cell in the periodic lattice. For example, in the PBG structure shown in Fig. 2, changing the radius of any rod/hole from the default value, or even removing one rod/hole, makes a local cavity or so called defect [23], [24]. Periodic defects in PC function as a low-loss waveguide, and the infinitesimal size of such structures is the key to the ultra-miniaturized delay lines. The group velocity of the light propagated in the defects can be controlled since it is inversely proportional to the coupling strength between the adjacent cavities [7].

A. Approximate Method to Find the Group Velocity

We propose an approximate method to find the group velocity of the transferring energy in coupled cavity configura-

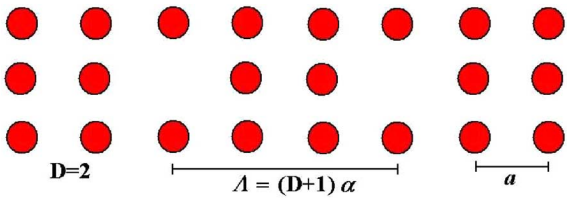

Fig. 14. Demonstration of two coupled cavities with $D = 2$.

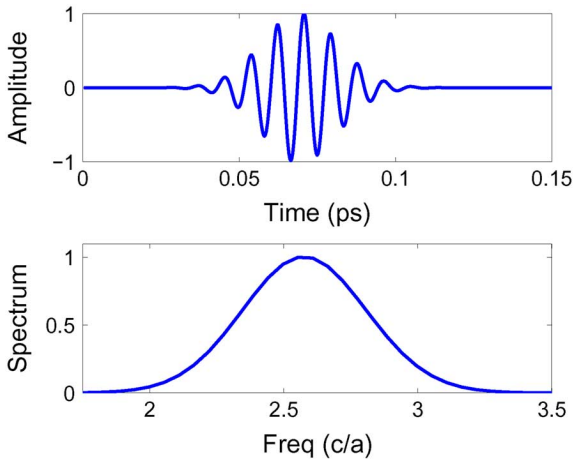

Fig. 15. Amplitude and spectrum of the source signal.

tions. Fig. 14 shows a narrow section of a PC lattice which contains two coupled cavities made by removing Si rods. As depicted in Fig. 14, D represents the number of rods between two cavities. We excite the first cavity with a wideband Gaussian modulated pulse and monitor the amplitude of the electric field at the center of the second cavity. Fig. 15 shows the amplitude and the spectrum of the source signal used to excite the first cavity. The input pulse spectrum is centered at $\lambda = 2.56a$, which is the resonance wavelength of a single cavity derived from the FDTD analysis. Next, we vary D from 1 to 6 and study the resonance phenomenon using FDTD simulation. After exciting the first cavity, the resonant E-field builds up immediately. Gradually the amplitude of the E-field decreases, because energy is coupling from the first cavity to the second one. Therefore, the E-field amplitude in the second cavity grows. This process continues until the E-field in the first cavity reaches its minimum value. Simultaneously, the E-field in the second cavity peaks. As time passes, the E-field shows a periodic behavior without any significant drop in its peak amplitude. Fig. 16 demonstrates the E-field at some point close to the middle of the second cavity versus time, for $D = 1$ to 4.

We define the *coupling period*, T_κ, as the required time for the complete transfer of the E-field from the first cavity to the second one. As the cavity spacing, D, increases the coupling period increases, which means energy needs a longer time to transfer. Table I presents the values of T_κ versus D. From Fig. 14 the center to center distance of two cavities, Λ, can be found as

$$\Lambda = (D+1) \cdot a \tag{5}$$

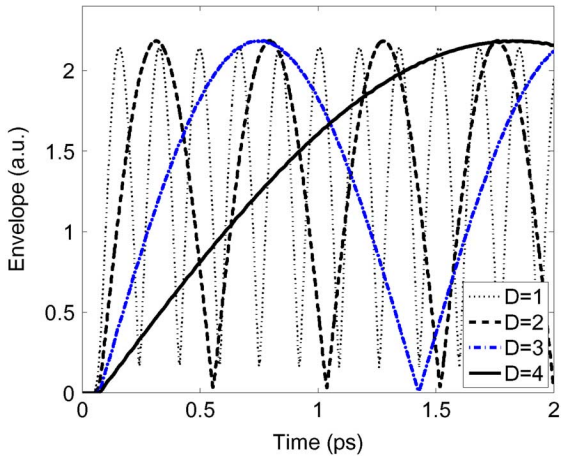

Fig. 16. Envelope of the E-field in the second cavity versus time for $D = 1, 2, 3$, and 4.

TABLE I
COUPLING PERIOD FOR TWO ADJACENT CAVITIES

Defect Spacing	Coupling Period(ps)
$D = 1$	0.09
$D = 2$	0.24
$D = 3$	0.69
$D = 4$	1.81
$D = 5$	4.60
$D = 6$	11.35

where a is the lattice constant. Therefore, we can define the *effective group velocity* for the energy transferring between two cavities, $v_{\rm ge}$ as

$$v_{\rm ge} = \frac{\Lambda}{T_\kappa}. \tag{6}$$

To compare the calculated effective group velocities with c, the speed of light, we define the *Miniaturization (Slowing)* Factor as $\mathrm{SF} = c/v_{\rm ge}$. Fig. 17 presents the calculated values of SF with this approximate method. The vertical axis of this graph is in Log-scale. We found an approximate exponential relation for SF, which could be the solution to a first-order differential equation

$$\mathrm{SF} = 12.75e^{[0.73(D-1)]}. \tag{7}$$

Numerical analysis of the large delay lines with large defect spacings is too time-consuming, but we can analyze a delay line with a small spacing and find the effective group velocity, using (5)–(7), to predict the time delay of larger structures.

B. Coupled Cavity Photonic Crystal Delay Line

Although reflective spiral delay line is the best option among other meandering line structures to obtain longer delay, but

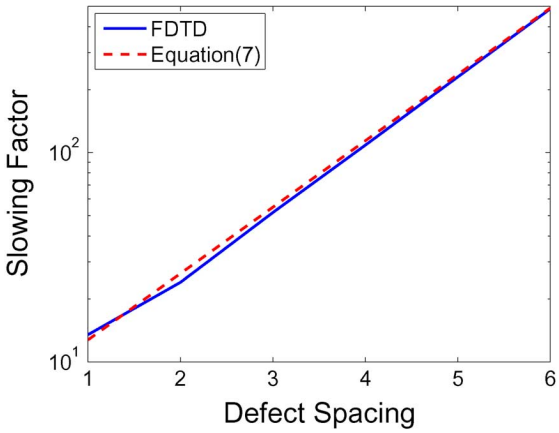

Fig. 17. Miniaturization (Slowing) Factor calculated from FDTD simulations.

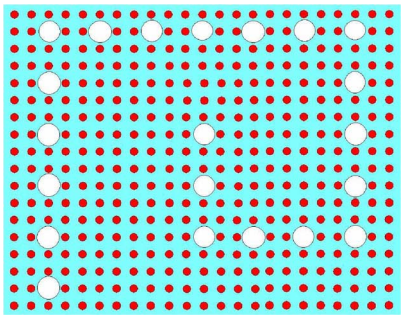

Fig. 18. Section of reflective spiral delay line made by coupled cavities with $D = 2$. Each white circle represents a missing rod.

crosstalk considerations prevents us to go further and achieve longer delays. For example, we cannot decrease the channel spacing. The only solution is to make the propagation of light slower. In Section IV-A we observed that the propagation of lightwave in PC coupled cavities is much slower than free space or Si, so if we replace the waveguide channels in Fig. 10 with coupled cavities, we should observe a significant increase in the delay. Fig. 18 shows how we can replace waveguide sections with coupled cavities. To prevent the fast coupling between parallel branches, the branch spacing must be greater than or equal to $2 \times \Lambda$. Our simulations show that energy can easily couple between the cavities at the corner and no mitering is required.

Following these instructions, for $D = 2$ we can insert 71 cavities in a 27 μm $\times$ 27 μm PC lattice, which are arranged in reflective spiral shape just like Fig. 18. Fig. 19 demonstrates the envelope of the input and reflected electric monitored at the first cavity of this delay line. It shows that the time delay has increased to 8.97 ps, whereas the loss is less than 0.05 dB. So, the other important feature of this delay line is its negligible loss.

For the coupled cavity delay line with $D = 2$ the defined figure of merit in (4) is $F_d = 100$, which indicates this structure decelerates light 100 times. The performance of this delay line is 4.5 times better than the waveguide delay line in Fig. 10, where F_d and time delay were respectively 22.2 and 1.99 ps. On the other hand, from Fig. 17 we find for $D = 2$, the slowing factor is 24. This slowing factor is 6.95 times more than the refractive

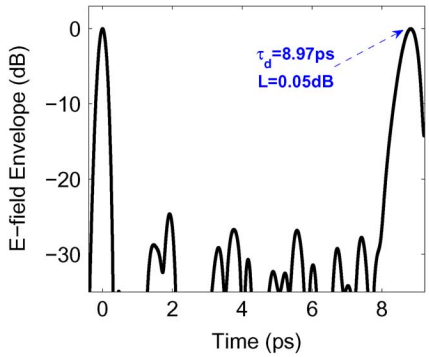

Fig. 19. Envelope of the electric recorded at the first cavity of a coupled cavity Si/Air reflective spiral delay line with $D = 2$.

index of Si ($n = 3.45$), which is indeed the slowing factor of Si medium. If we assume the effective refractive index of the waveguide delay line is the same as that of Si, we expect the coupled cavity delay line to generate a delay of 13.85 ps. One reason for this discrepancy is that the net length of the coupled cavity chain in the current delay line is less that the net length of the waveguide channels in Fig. 10. As we mentioned in Section II-C, the spacing between waveguide channels is equal to five rows of Si rods but as we see in Fig. 18 the spacing between the parallel cavity branches is equal to eight rods. Therefore, we should consider the effect of net length of delay lines when we want to compare time delays of different structures.

Considering the results of the approximate method for finding the effective group velocity, if we increase the cavity spacing to 3, the time delay will increase 2.14 times.

V. Conclusion

We introduced the reflective spiral delay line, which produces the longest delay, lowest transmission loss and least crosstalk noise in comparison with classical delay line structures. We used the widest bandgap criterion for selecting PC lattice parameters, and studied the effects of channel length and spacing on the crosstalk to find the proper values which reduce the crosstalk. The delay generated by the reflective spiral line is almost uniform over the required microwave bandwidths and will change by a considerable shift in the optical wavelength. Thus, it is possible to design a tunable delay line without distorting the characteristics of the microwave signal. Furthermore, we proposed an approximate method to find the group velocity of lightwave energy transferring between coupled cavities in PC, and demonstrated that by introducing coupled cavities in the reflective spiral structure, the delay increases by almost a factor of five, which corresponds to the propagation of lightwave 100 times slower than free space. Finally, we noted that an important feature of the coupled cavity delay line is its low loss, and by increasing the cavity spacing we obtain longer time delays.

References

[1] C. Chang, D. Altman, D. Wehner, and D. Albares, "Noncoherent radar moving target indicator using fiber optic delay lines," *IEEE Trans. Circuits Syst.*, vol. CS-26, no. 12, pp. 1132–1135, Dec. 1979.

[2] B. Ortega, J. Cruz, J. Capmany, M. Andres, and D. Pastor, "Analysis of a microwave time delay based on a perturbed uniform fiber Bragg grating operating at constant wavelength," *J. Lightw. Technol.*, vol. 18, no. 3, pp. 430–436, Mar. 2000.

[3] S. Nishikawa, S. Lan, N. Ikeda, Y. Sugimoto, H. Ishikawa, and K. Asakawa, "Optical characterization of photonic crystal delay lines based on one-dimensional coupled defects," *Opt. Lett.*, vol. 27, no. 23, pp. 2079–2081, Dec. 2002.

[4] S. Mookherjea, "Dispersion characteristics of coupled-resonator optical waveguides," *Opt. Lett.*, vol. 30, no. 18, pp. 2406–2408, 2005.

[5] Y. Jiang, B. Howley, Z. Shi, Q. Zhou, R. Chen, M. Chen, G. Brost, and C. Lee, "Dispersion-enhanced photonic crystal fiber array for a true time delay structured x-band phased array antenna," *IEEE Photonics Tech. Lett.*, vol. 17, pp. 187–189, 2005.

[6] Z. Wang and S. Fan, "High-performance optical code generation and recognition by use of a 511-chip, 640-gchip/s phase-shifted superstructured fiber Bragg grating," *Opt. Lett.*, vol. 30, no. 4, pp. 355–357, Feb. 2005.

[7] J. K. S. Poon, J. Scheuer, Y. Xu, and A. Yariv, "Designing coupled resonator optical waveguide delay lines," *OSA J. Opt. Soc. Amer. B*, vol. 21, pp. 1665–1673, 2004.

[8] S. Lan, S. Nishikawa, H. Ishikawa, and O. Wada, "Design of impurity band-based photonic crystal waveguides and delay lines for ultrashort optical pulses," *J. Appl. Phys.*, vol. 90, no. 9, pp. 4321–4327, Nov. 2001.

[9] J. Liu, B. Shi, D. Zhao, and X. Wang, "Optical delay in defective photonic bandgap structures," *J. Opt. A: Pure Appl. Opt.*, vol. 4, no. 6, pp. 636–639, Nov. 2002.

[10] M. Povinelli, S. Johnson, and J. Joannopoulos, "Slow-light, band-edge waveguides for tunable time delays," *Opt Express* vol. 13, no. 18, pp. 7145–7159, 2005 [Online]. Available: http://www.opticsexpress.org/abstract.cfm?id=85390

[11] M. Fakharzadeh, O. Ramahi, S. Chaudhuri, and S. Safavi-Naeini, "Miniaturized optical delay lines using photonic crystals," in *Proc. IEEE Inernational Microwave Symp.*, San Francisco, CA, USA, 2006, pp. 10–13.

[12] S. G. Johnson, P. R. Villeneuve, S. Fan, and J. D. Joannopoulos, "Linear waveguides in photonic-crystal slabs," *Phys. Rev. B*, vol. 62, pp. 8212–8222, 2000.

[13] V. Italia, M. Pisco, S. Campopiano, A. Cusano, and A. Cutolo, "Chirped fiber Bragg gratings for electrically tunable time delay lines," *IEEE J. Sel. Topics Quantum Electron.*, vol. 11, no. 2, pp. 408–416, Mar./Apr. 2005.

[14] M. Koshiba, "Wavelength division multiplexing and demultiplexing with photonic crystal waveguide couplers," *IEEE J. Lightw. Technol.*, vol. 19, no. 12, pp. 1970–1975, Dec. 2001.

[15] S. Boscolo, M. Midrio, and C. G. Someda, "Coupling and decoupling of electromagnetic waves in parallel 2-D photonic crystal waveguides," *IEEE J. Quantum Electron.*, vol. 38, no. 1, pp. 47–53, Jan. 2002.

[16] S. Kuchinsky, V. Y. Golyatin, A. Y. Kutikov, T. P. Pearsall, and D. Nedeljkovic, "Coupling between photonic crystal waveguides," *IEEE J. Quantum Electron.*, vol. 38, no. 10, pp. 1349–1352, Oct. 2002.

[17] W. Kuang, W. J. Kim, A. Mock, and J. D. O'Brien, "Propagation loss of line-defect photonic crystal slab waveguides," *IEEE J. Sel. Topics Quantum Electron.*, vol. 12, no. 6, pp. 1183–1195, Nov./Dec. 2006.

[18] M. Fakharzadeh, O. Ramahi, S. Chaudhuri, and S. Safavi-Naeini, "A photonic crystal delay line with two time delays," in *Proc. 36th Eur. Microwave Conf.*, Manchester, U.K., Sept. 10–15, 2006, pp. 1383–1386, 2006.

[19] A. Huttunen, T. Koponen, and P. Törmä, "Conditions for waveguide decoupling in square-lattice photonic crystals," *J. Appl. Phys.*, vol. 96, pp. 4039–0, 2004.

[20] A. Mekis, J. C. Chen, S. Fan, P. R. Villeneuve, and J. D. Joannopoulos, "High transmission through sharp bends in photonic crystal waveguides," *Phys. Rev. Lett.*, vol. 77, pp. 3787–3790, 1996.

[21] J. D. Joannopoulos, R. D. Meade, and J. N. Winn, *Photonic Crystals: Molding the Flow of Light*. Princeton, NJ: Princeton Univ. Press, 1995.

[22] X. Wang, Z. Wang, and S. Fran, "Optical circulators in two-dimensional magneto-optical photonic crystals," *Opt. Lett.*, vol. 30, no. 15, pp. 1989–1991, 2005.

[23] D. R. Smith, R. Dalichaouch, N. Kroll, S. Schultz, S. L. McCall, and P. M. Platzman, "Photonic band structure and defects in one and two dimensions," *J. Opt. Soc. Amer. B, Opt. Phys.*, vol. 10, no. 2, pp. 314–321, Feb. 1993.

[24] S. Fan, J. Winn, A. Devenyi, J. C. Chen, R. D. Meade, and J. D. Joannopoulos, "Guided and defect modes in periodic dielectric waveguides," *J. Opt. Soc. Am. B*, vol. 12, pp. 1267–1272, 1995.

Mohammad Fakharzadeh was born in Abadan, Iran, on December 25, 1978. He received the B.Sc. degree in electrical engineering (honors) from Shiraz University, Shiraz, Iran and the M.Sc. degree in electrical engineering (telecommunications) from Sharif University of Technology, Tehran, Iran, in 2000 and 2002, respectively.

In January 2003, he joined the Department of Electrical Engineering at Chamran University of Ahvaz as the youngest faculty member, where he was evaluated as the best instructor by undergraduate students. In September 2004, he joined the RF, Microwave and Photonics Group at the Electrical and Computer Engineering Department, the University of Waterloo, Waterloo, ON, Canada. His areas of interest include nanophotonics, optical delay lines and coupled cavity structures, beamforming of phased array systems, radar systems, and adaptive filters.

Omar M. Ramahi received the B.S. degrees in mathematics and electrical and computer engineering (summa cum laude) from Oregon State University, Corvallis, OR. He received the M.S. and Ph.D. degrees in electrical and computer engineering from the University of Illinois, Urbana-Champaign.

From 1990 to 1993, he held a visiting fellowship position at the University of Illinois, Urbana-Champaign. From 1993 to 2000, he worked at Digital Equipment Corporation (presently, HP), where he was member of the alpha server product development group. In 2000, he joined the faculty of the James Clark School of Engineering, University of Maryland, College Park, as an Assistant Professor and later as a tenured Associate Professor. At the University of Maryland, he was also a faculty member of the CALCE Electronic Products and Systems Center. Presently, he is the Associate NSERC/RIM Industrial Research Chair in the Electrical and Computer Engineering Department, University of Waterloo, Waterloo, ON, Canada. He was instrumental in developing computational techniques to solve a wide range of electromagnetic radiation problems in the fields of antennas, high-speed devices and circuits and EMI/EMC. His interests include experimental and computational EMI/EMC studies, high-speed devices and interconnects, biomedical applications of electromagnetics, novel optimization techniques, and interdisciplinary studies linking electromagnetic application to novel materials. He has authored and coauthored over 150 journal and conference paper. He is a coauthor of the book EMI/EMC Computational Modeling Handbook, 2nd Ed. (Springer-Verlag, 2001). He served as a consultant to several companies and was a cofounder of EMS-PLUS, LLC and Applied Electromagnetic Technology, LLC.

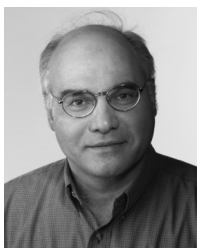

Safiedin Safavi-Naeini received the B.Sc. degree in electrical engineering, from University of Tehran, Tehran, Iran, 1974 and the M.Sc. and Ph.D. degrees in electrical engineering, both from University of Illinois, Champaign-Urbana, in 1975 and 1979, respectively.

He joined the University of Waterloo, Waterloo, ON, Canada, in 1996, where he is now a Professor at the Department of Electrical and Computer Engineering and holds the RIM/NSERC Industrial Research Chair in Intelligent Radio/Antenna and Photonics. He has more than 25 years of research experience in antenna, RF/microwave technologies, integrated photonics, and computational electromagnetics. He has published more than 60 journal publications and 150 conference papers in international conferences. He has led several international collaborative research programs with research institutes in Germany (DAAD fund), Finland (Nokia), Japan, China (BVERI, Institute of Optics), and USA,

which have resulted in novel technologies and efficient design methodologies. He has been scientific and technical consultant to many North American, European, and Asian international companies.

Sujeet K. Chaudhuri was born in Calcutta, India, on August 25, 1949. He received the B.E. (honours) degree in electronics engineering from BITS/Pilani, the M.Tech. degree in electrical communication engineering from IIT/Delhi, India, in 1970 and 1972, respectively, and the M.A.Sc. degree in microwave engineering and the Ph.D. degree in electromagnetic theory the University of Manitoba, Winnipeg, MB, Canada, in 1973 and 1977, respectively.

In 1977, he joined the University of Waterloo, Waterloo, ON, Canada, where he is currently a Professor and the O'Donovan Research Chair in the Electrical and Computer Engineering Department. He was the Chair of Electrical and Computer Engineering Department from 1993 to 1998 and the Dean of the Engineering Faculty from 1998 to 2003. He has also held a Visiting Associate Professor position in the Electrical Engineering and Computer Science Department of the University of Illinois, Chicago, during the years 1981 and 1984, a visiting Professorship at the National University of Singapore in 1990–1991, and a Erskine Fellowship at the University of Canterbury, New Zealand, in 1998. He visited the Korea Advanced Institute of Science and Technology (KAIST) as a BK-21 International Fellow, and the Pohang University of Science and Technology (POSTECH), Korea as a International Visiting Professor in 2004 and 2005, respectively. He has been involved in Contract Research and Consulting Work with several Canadian and U.S. industries and government research organizations. His current research interests are in guided-wave/electro-optic structures, planar microwave structures, dielectrc resonators, optical and EM computational modelling and the photonic integrated circuits based on emerging materials and technologies.

Dr. Chaudhuri is a member of URSI Commission B, and Sigma Xi.